OPEN ACCESS
IOP Publishing
Metrologia
Metrologia **57** (2020) 055010 (12pp)
https://doi.org/10.1088/1681-7575/ab8d7b

Artifacts and errors in cross-spectrum phase noise measurements

Yannick Gruson[1], Adrian Rus[2], Ulrich L Rohde[3,4], Alexander Roth[5] and Enrico Rubiola[1,6,7]

[1] FEMTO-ST Institute, UBFC CNRS Besançon France.
[2] Independent researcher, Bucharest, Romania. Call sign YO3HHZ.
[3] Synergy Microwave Corp. Paterson NJ United States of America. Call sign N1UL.
[4] Universität der Bundeswehr München Germany.
[5] Rohde & Schwarz München Germany.
[6] Istituto Nazionale di Ricerca Metrologica INRiM Torino Italy.
[7] Reference author

E-mail: rubiola@femto-st.fr

Received 30 December 2019, revised 22 April 2020
Accepted for publication 27 April 2020
Published 19 August 2020

Abstract

This article deals with the erratic and inconsistent phase-noise spectra often seen in low-noise oscillators, whose floor is of the order of −180 dBc/Hz or less. Such oscillators are generally measured with two-channel instruments based on averaging two simultaneous and statistically independent measures. Our new method consists of inserting a dissipative attenuator between the oscillator under test and the phase-noise analyzer. The thermal noise of the attenuator introduces a controlled amount of phase noise. We compare the phase noise floor to the theoretical expectation with different values of the attenuation in small steps. The analysis reveals a negative bias (underestimation of phase noise) due to the thermal energy of the internal power splitter at the instrument input, and an uncertainty due to crosstalk between the two channels. In not-so-rare unfortunate cases, the bias results in a negative phase-noise spectrum, which is an obvious nonsense. Similar results are observed separately in three labs with instruments from the two major brands. We provide experimental evidence, full theory and suggestions to mitigate the problem, and a first attempt to assess the uncertainty. Our multiple-attenuators method provides quantitative information about the correlation phenomena inside the instrument.

Keywords: phase noise, oscillator (RF, microwave), frequency stability, noise, instrumentation

(Some figures may appear in colour only in the online journal)

1. Introduction

Modern analyzers measure the phase noise (PN, or PM noise) by correlation and averaging on the simultaneous measurement of the oscillator under test (DUT) with two separate channels, each consisting on a phase detector and a frequency reference. The DUT noise is extracted after rejecting the background noise of the instrument, assuming that the two channels are statistically independent. After the seminal paper [1], and the early application shown in [2], this choice is adopted by virtually all manufacturers (table 1). The dual channel scheme comes in two flavors, with one or two reference oscillators. We focus on the latter because it enables the noise rejection of the reference oscillators, and also of the frequency synthesizers which may be interposed between reference oscillators and phase detectors.

The correlation-and-averaging process rejects the single-channel noise proportionally to $1/\sqrt{m}$, where m is the number of averaged spectra, that is, 5 dB per factor-of-ten. Nowadays,

Table 1. Dual-Channel Phase Noise Analyzers.

Brand	Type or Series
AnaPico	APPH series
Berkeley Nucleonics Corp.	7000 series
Holzworth	HA7062 series
Jackson Labs Technologies	PhaseStation 53 100A
Keysight Technologies	E5500 series
Microsemi Corporation	3120A / 5120A
NoiseXT	DCNTS / NXA
OEwaves	HI-Q TMS
Rohde & Schwarz	FSWP series

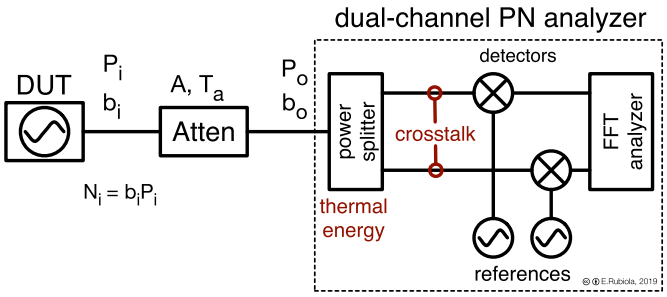

Figure 1. Block diagram of the experiment.

digital electronics provides a high computing power and memory size for cheap, as compared to the cost and to the complexity of RF and microwave technology. Thus, the theoretical rejection can exceed 30 dB if the experimentalist accepts the long measurement time it takes, ultimately limited by the time-frequency indetermination theorem. However, such rejection cannot be achieved in practice because of fundamental phenomena and artifacts. The thermal energy in the input power splitter [3–7] and impedance matching [8] first caught the attention of the scientific community. These and other problems were addressed in three international workshops [9–11].

Most practitioners, naively, believe that a noise analyzer always *over-estimates* the DUT noise because it *adds* its own background noise. This is not true in the case of the two-channel instruments because the cross spectrum is the frequency-domain equivalent of the covariance. The correlation between channels introduces systematic errors and artifacts, which can be positive or negative. The consequence is that there is no a-priori rule to state whether the instrument over-estimates or under-estimates the DUT noise. A problem is that the noise rejection due to averaging, usually calculated and displayed together with the phase noise, does not account for artifacts and systematic errors. Another problem is that the instruments display the absolute value of the cross spectrum, giving no warning about negative outcomes. The combination of these facts originates erratic and misleading results.

We propose an experiment (figure 1) that reveals the presence systematic errors due to unwanted correlated terms. We focus on the 100 MHz OCXOs because this type of oscillator exhibits the lowest white PM noise floor. However trivial the experiment may seem, nothing even broadly similar has been reported in the literature. We provide all the details related to two specific cases, together with the full theoretical interpretation.

2. Phase noise and thermal energy

Let us start with a review of key facts, based on References [3–7]. The phase noise is described in terms the power spectral density (PSD) of the random phase $\varphi(t)$, and denoted with $S_\varphi(f)$. A model that is found useful to describe oscillators and components is the polynomial law

$$S_\varphi(f) = \sum_{n\le -4}^{0} \mathsf{b}_n f^n [\mathrm{rad}^2/\mathrm{Hz}] \ , \tag{1}$$

where the term b_0 is the white PM noise, b_{-1}/f is the flicker PM noise, b_{-2}/f^2 is the white FM noise, b_{-3}/f^3 is the flicker FM noise, b_{-4}/f^4 is the frequency random walk, and other terms can be added. The quantity $\mathscr{L}(f)$, most often used by the manufacturers, is defined as $\mathscr{L}(f) = (1/2)S_\varphi(f)$ [12]. As a matter of fact, white phase noise is mostly of additive origin. Accordingly, it can be written as

$$\mathsf{b}_0 = \frac{N}{P} \ , \tag{2}$$

where P is the carrier power, and N is the power spectral density (PSD) of the RF noise. In this context, we prefer the unit W/Hz to J. By analogy with the PSD $N = kT$ of the thermal noise, we associate to b_0 the equivalent temperature

$$T = \frac{P\mathsf{b}_0}{k}, \tag{3}$$

where $k = 1.380\,649\times10^{-23}$ J/K (exact) is the Boltzmann constant.

2.1. The effect of the attenuator

Physical insight suggests that the dissipative attenuator can only degrade the signal-to-noise ratio (SNR), which results in increased PM noise. Focusing on the white noise at the attenuator in and out, we use the subscripts 'i' and 'o' dropping the subscript 0. For example, b_i stands for b_{0i}, and b_o for b_{00}. Thus (2) rewrites as $\mathsf{b}_i = N_i/P_i$, or $\mathsf{b}_o = N_o/P_o$. Assuming that everything is matched to the characteristic impedance R_0, the RF white noise at the attenuator output is

$$N_o = kT_iA^2 + kT_a\left(1 - A^2\right) \ , \tag{4}$$

where kT_i is the input noise, A is the voltage gain of the attenuator, $A^2 < 1$, and T_a is the temperature of the attenuator. The term kT_iA^2 means that the input noise kT_i is attenuated by the factor A^2, like any signal. The term $kT_a(1 - A^2)$ is the thermal noise added by the attenuator. This is obvious if one replaces the oscillator with a resistive load R_0 at the temperature T_a. In this condition the output is equivalent to a resistor R_0 at the temperature T_a. Thus, the total output noise is kT_a, independent of A. Equation (4) is well known in radio astronomy, where

it finds application in the estimation of the effect of losses in the antenna and in the line between antenna and receiver [13, section 7-2b (Noise Temperature of an Attenuator)], and in the calibration of the receiver [14, section 4.2.4 (Receiver Calibration)].

After (2)–(4), the white PM noise at the attenuator output is

$$\mathsf{b}_o = \frac{kT_i}{P_i} + \frac{kT_a\left(1-A^2\right)}{A^2P_i}, \tag{5}$$

which is obviously greater than $\mathsf{b}_i = kT_i/P_i$.

3. Inside the dual-channel noise analyzer

3.1. The cross-spectrum estimator

The cross-spectrum estimator is a general tool. Here, it finds application to two key signals inside the instrument: (i) the voltage at the outputs of the power splitter, and (ii) the phase at the output of the detectors (Figure: 1). Let us start with

$$x(t) = a(t) + c(t) \tag{6}$$

$$y(t) = b(t) + c(t) \tag{7}$$

where $a(t)$ and $b(t)$ are the background noise of the channel $\mathcal{A}$ and $\mathcal{B}$. They are statistically independent, and have zero mean and equal or similar variance. The signal $c(t)$ is the target, that is, the DUT noise. Thus, the statistical properties of $c(t)$ are measured after averaging out $a(t)$ and $b(t)$. As said, (6)–(7) apply to the RF signal or to the PM noise, at choice. Thus, we can measure the RF spectrum [W/Hz], or the PM noise spectrum [rad^2/Hz]. The reader interested to know more about the method should refer to [15], [16] and [2].

As a mathematical concept, the cross PSD is defined as the Fourier transform of the autocorrelation function. However, under certain conditions which are generally met in the case of physical signals digitized on a finite acquisition time T, it can be evaluated using the Fourier transforms. Thus, denoting the discrete Fourier transform with the uppercase letter, as in $X(f) \leftrightarrow x(t)$, the one-sided cross PSD is evaluated as

$$S_{yx}(f) = \frac{2}{T}\left[Y(f)X^*(f)\right] . \tag{8}$$

The denominator T is the acquisition time, the superscript '*' means complex conjugate, and the factor '2' accounts for energy conservation after suppressing the negative frequencies. Equation (8) states a general fact, thus it holds for one realization, for the average or for the expectation, depending on the context. Dropping the frequency and expanding $X = A + C$ and $Y = B + C$ we get

$$S_{yx} = \frac{2}{T}\left(B+C\right)\left(A^*+C^*\right) . \tag{9}$$

The mathematical expectation $\mathbb{E}\{S_{yx}\}$ is

$$\mathbb{E}\{S_{yx}\} = \frac{2}{T}\mathbb{E}\{CC^*\} = \mathbb{E}\{S_c\} \tag{10}$$

because $\mathbb{E}\{BA^*\} = 0$, $\mathbb{E}\{BC^*\} = 0$, and $\mathbb{E}\{CA^*\} = 0$. All the useful information is in CC^*, thus $S_c > 0$. By contrast, all the background noise goes in BA^*, BC^* and CA^*, and under normal circumstances it is equally distributed between real and imaginary part. It is therefore clear that the optimum estimator is

$$\widehat{S_{yx}} = \Re\left\{\langle S_{yx}\rangle_m\right\} . \tag{11}$$

This estimator has two important properties, (i) it is unbiased, and (ii) it is the fastest because it takes in the smallest amount of background noise. A problem with $\Re\left\{\langle S_{yx}\rangle_m\right\}$ is that it is not always positive before averaging out the background noise, or in the presence of spurs. The negative outcomes cannot be plotted on a logarithmic scale (dB). The FSWP [17, equation (4)] uses the estimator

$$\widehat{S_{yx}} = \left|\langle S_{yx}\rangle_m\right| . \tag{12}$$

Albeit the documentation provided by other manufacturers gives little indication about the estimator, we believe that (12) is the most chosen option. A reason is that it shows no negative values, thus it is always suitable to be represented on a log scale. Another reason is that such estimator is positively biased, and the bias decreases monotonically as m increases. Thus, under normal circumstances $\left|\langle S_{yx}\rangle_m\right|$ converges to $\mathbb{E}\{S_c\}$, after decreasing monotonically during the measurement process. The estimator (12) matches the behavior we observe in the regular use of the instruments, where no attenuator is inserted at the input. Now we break the hypothesis of statistically independent channels, and we introduce the disturbing signal $d(t) \leftrightarrow D(f)$, the same in the two channels but for the sign, $\varsigma_x = \pm 1$ and $\varsigma_y = \pm 1$, as we did in [18]

$$X = A + C + \varsigma_x D \tag{13}$$

$$Y = B + C + \varsigma_y D , \tag{14}$$

The signal D is either correlated or anticorrelated. Introducing $\varsigma = \varsigma_x\varsigma_y = \pm 1$, and expanding $\mathbb{E}\{S_{yx}\}$ as above, we find

$$\mathbb{E}\{S_{yx}\} = \mathbb{E}\{S_c\} + \varsigma\mathbb{E}\{S_d\} . \tag{15}$$

Thus, ς is the sign of the correlation coefficient, and the term $\varsigma\mathbb{E}\{S_d\}$ is a systematic bias, positive or negative. A substantially equivalent approach is found in [5, section II], which differs in the analysis of four separate cases (the presence or not of the disturbing signal $d(t)$, and the sign of the correlation), instead of the compact form (13)–(14) and (15). The disturbing signal can be (i) the thermal energy in the input power splitter (section 3.2), (ii) the crosstalk between the two channels (section 5.1), and (iii) the AM noise pickup [19], or other effects not considered here.

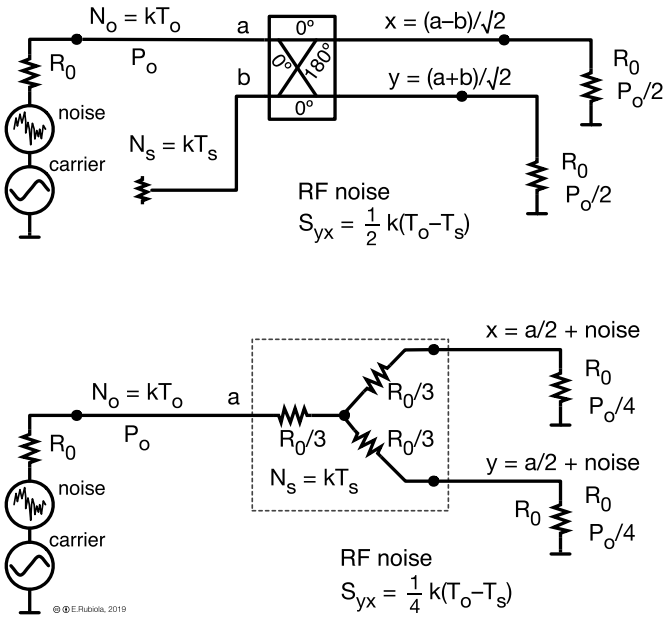

Figure 2. Signal and noise model of the most common power splitters. The reactive power splitter (top) is free from dissipation, thus it has 3 insertion loss. The resistive power splitter (bottom) has 6 dB insertion loss.

3.2. Application to the input power splitter

Two types of power splitters are mostly used, shown on figure 2. The loss-free splitter is a 3 dB directional coupler terminated at one input (dark port). The resistive splitter is a Y network which attenuates the input signal by 6 dB. Here, $x(t)$ and $y(t)$ are the RF voltages at the output of the power splitter. Denoting with T_o the equivalent noise temperature at the power-splitter input, and with T_s the temperature of the splitter, trite calculation shows that the correlated noise is

$$\mathbb{E}\{S_{yx}\} = \frac{1}{2}k\Big(T_o - T_s\Big) \tag{16}$$

for the 3-dB dissipation-free coupler. Interestingly, (16) is a classical result from Johnson thermometry [20, 21], with well known application in microwaves [22, 23].

Similarly, we find

$$\mathbb{E}\{S_{yx}\} = \frac{1}{4}k\Big(T_o - T_s\Big) \tag{17}$$

for the 6-dB resistive coupler. Deriving (16) and (17) from (15), ς does not need to appear explicitly because it always hold that $\varsigma = -1$. Because the output power is $P_o/2$ for the 3-dB splitter and $P_o/4$ for the 6-dB splitter, the output SNR is the same, and the white PM noise is

$$\mathbb{E}\{\mathsf{b}_o\} = \frac{k(T_o - T_s)}{P_o} \,. \tag{18}$$

Reference [6, section IV] provides an extension to other less common types of power splitter.

3.3. Hardware architectures

The FSWP [17, 24] is based on the SDR (Software Defined Radio) technology after down-converting the input to an appropriate IF (see [25] for a modern treatise of SDR). The mixers are used in the linear region because linearity prevents the AM noise from polluting the phase noise measurement. The use of I-Q mixers enables to unwrap the phase, and to measure beyond the IF. Two operating modes are used, depending on the Fourier frequency. Up to 1 MHz, the input RF signal is down converted to 1.3 MHz. Beyond 1 MHz, the reference synthesizers are set close to the input frequency, keeping the beat note below 10 Hz. In both cases, I and Q of the down-converted signal are digitized, and the phase information is extracted in FPGA. The FSWP uses a 3-dB coupler as the input power splitter (actually, three different couplers are switched, for < 1 GHz, $1 - 8$ GHz, and $8 - 50$ GHz).

The E5052B [26] is based on direct phase detection with double-balanced mixers as the phase-to-voltage converters. The mixers are saturated at both inputs, and driven with synchronous signals kept in quadrature. The mixer output is digitized and processed. The power splitter is a Y resistive network.

In both cases, the signals $x(t)$ and $y(t)$ used to calculate $\widehat{S_{yx}(f)}$ are the instantaneous phases at the detector output, sampled and digitized. This is the case of all the spectra (figures 3, 5, 6 and 8) and the coefficient b_0 (figure 4 and 7).

4. Experiments and results

The experiment consists of the measurement of the white noise floor after inserting various dissipative attenuators in the path from the oscillator under test to the phase noise analyzer, as shown on figure 1.

Two oscillators are tested, $\mathcal{A}$ a Wenzel 501-04623E, and $\mathcal{B}$ a Wenzel 501-25900B 'Golden Citrine,' both 100-MHz OCXOs intended for the lowest-noise applications. The former dates more than 20 years ago. The latter is the top low-PM-noise oscillator by Wenzel. After comparing to the spectra published on the web pages of several manufactures, $\mathcal{B}$ is the OCXO that exhibits the lowest white noise we have found, below -190 dBc/Hz [27].

The oscillator is clamped on a vibration-damping breadboard, of the same type commonly seen in optical experiments. A 150-MHz low-pass filter (MiniCircuits SLP-150) is inserted at the oscillator output. The attenuation is obtained by stacking small-size SMA attenuators at the filter output, close to the oscillator. The attenuators (Radiall brand) are intended for DC to 18 GHz. In most of the tests, the phase-noise analyzer is a Rohde Schwarz FSWP 26 with high-stability OCXO and cross-spectrum options. The phase-noise analyzers are referenced to a T4Science Hydrogen maser, in turn monitored vs other masers of the same type. The power is measured with a Rohde & Schwarz power meter, which replaces temporarily the phase-noise analyzer before each measurement. The attenuation is evaluated as the power ratio. All the experiments are done in a Faraday cage with usual isolation transformer and EMI filters. Temperature and humidity are stabilized to

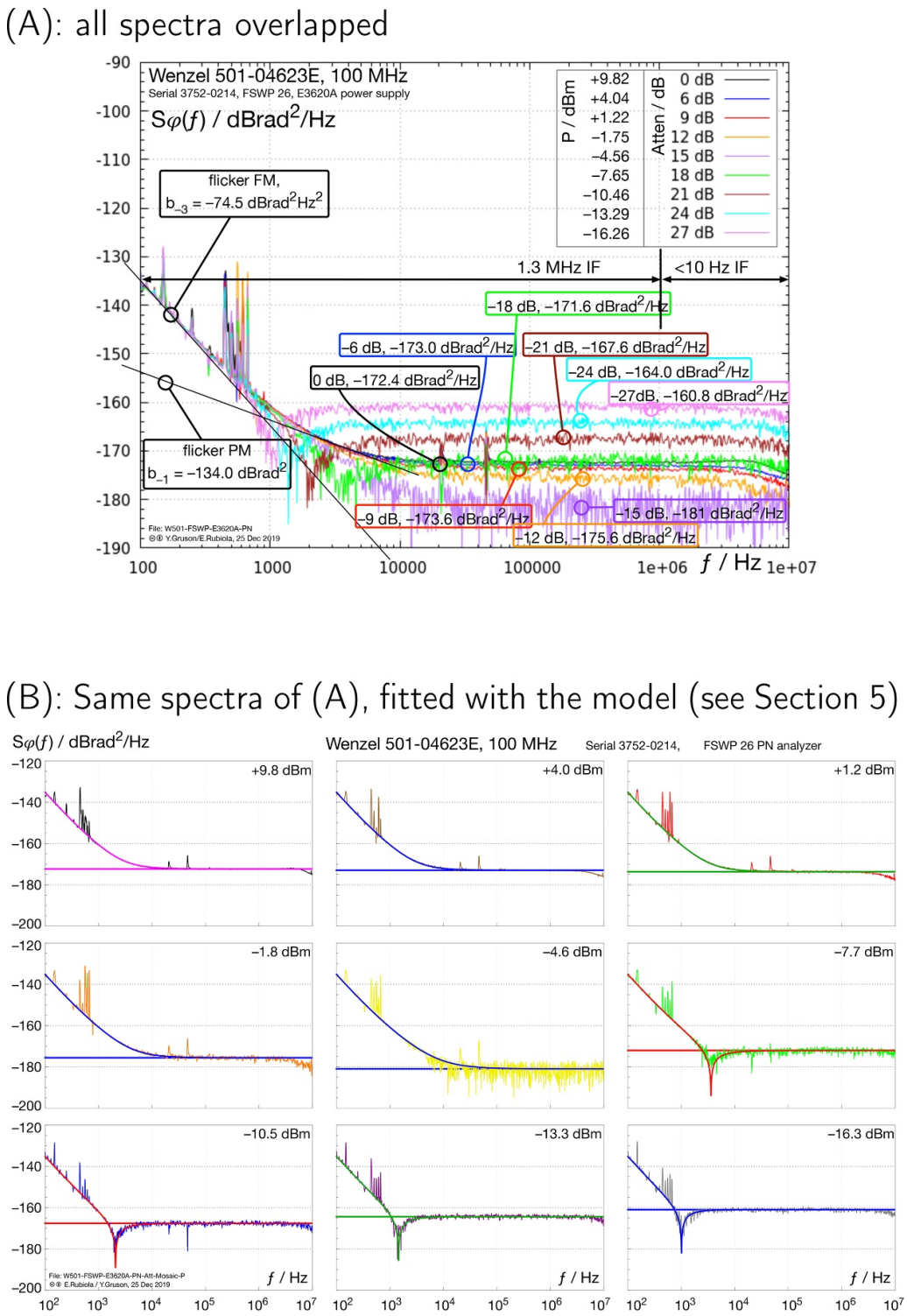

Figure 3. Phase noise of the Wenzel 501-04 623E OCXO measured with the FSWP 26.

$22 \pm 0.5\,^{\circ}\mathrm{C}$ and $50\,\% \pm 10\,\%$ by a PID control, which also guarantee a drift smaller than 0.2 K/hour. The environment control is probably overdone for PM noise measurements, yet it helps to get conservative results.

Figure 3 shows the phase noise spectra of the oscillator $\mathcal{A}$, observed with different values of the attenuation between 0 dB and 27 dB. The experimental data (dots) on figure 4 are the white PM noise from figure 3, averaged on a suitable region 2–3 decades wide. Surprisingly, the observed floor does not match the 'attenuator only' plot. The latter is calculated from (5). Instead, the floor decreases monotonically from 0 dB to 15 dB attenuation, and it increases monotonically beyond.

Measuring the oscillator $\mathcal{A}$ with a Keysight E5052B, we see that the white PM noise decreases monotonically with the

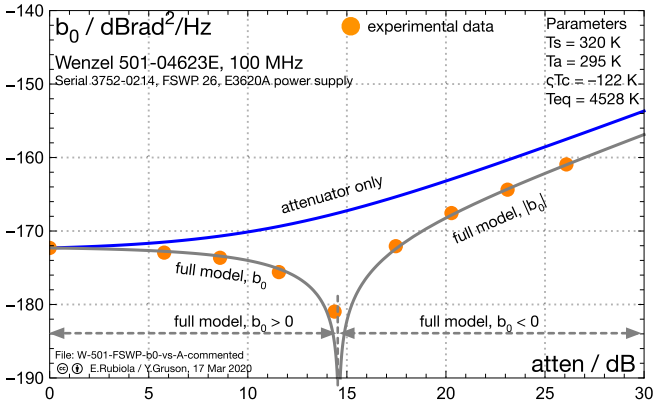

Figure 4. White noise floor b_0 (dots) taken from figure 3-A, compared to the 'attenuator only' model based on (5). The 'full model' plot and the parameters are discussed in section 5.

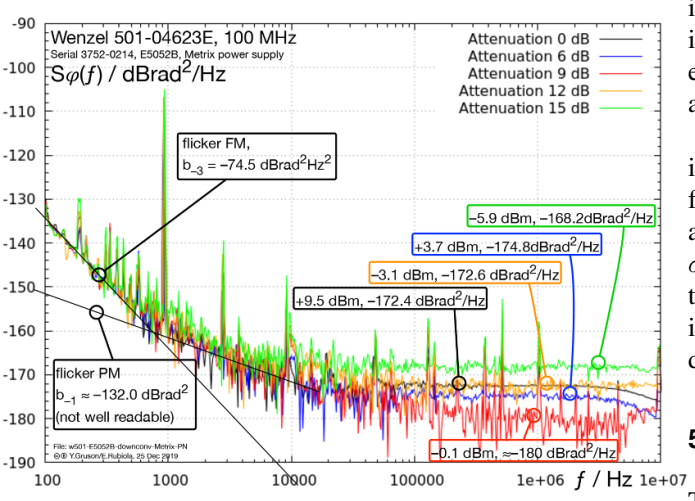

Figure 5. Phase noise spectrum of the same oscillator of figure 3, measured with a Keysight E5052B phase noise analyzer.

attenuation, attends a minimum at 9 dB, and increases at higher attenuation (figure 5). We could not push the attenuation beyond 15 dB because the carrier power falls below the minimum for the E5052B.

The anomalously low white PM noise when an attenuator is introduced was first observed by one of us (AR) in his radio amateur lab at home, measuring a Wenzel 501-04538F 10 MHz OCXO with a FSWP 8.

Comparing figure 5 to figure 3(A), the calibration of the two instruments is consistent within at most a small fraction of a dB. The flicker of frequency is the same, $\mathsf{b}_{-3} = -74.5$ dB rad^2 Hz^2. Likewise, the white noise floor at 0 dB attenuation is the same, $\mathsf{b}_0 = -172.4$ dB rad^2/Hz. The 2-dB discrepancy in the flicker PM noise is not significant because the b_{-1} coefficient is hardly readable on figure 5.

Figure 3(B) shows the same plots of figure 3(A), just separated for better readability. The most interesting fact is the appearance of dips at 1–1.5 kHz for attenuation of ≥ 18 dB.

Figures 6 and 7 refer to the same experiment of figures 3 and 4, but for the oscillator $\mathcal{B}$. In this case the white noise floor increases monotonically with the attenuation, but there is a significant discrepancy between the experimental data and the 'attenuator only' floor predicted by (5). Additionally, dips are seen on figure 6(B) at 2–20 kHz, more noticeable than on figure 3(B).

Inspired by the theory (section 3.1), we hacked a FSWP at the Rohde Schwarz R&D facility in München, extracting $\Re\{\langle S_{yx}(f)\rangle\}$ and $\Im\{\langle S_{yx}(f)\rangle\}$. This instrument is of the same type of that we have in Besançon. In München we measured a third oscillator $\mathcal{C}$, a 100-MHz Wenzel 501-25 900B 'Golden Citrine' OCXO, same brand and type of $\mathcal{B}$. The DUT is connected via a 3-dB attenuator, and the FSWP had internal 5-dB attenuation mechanically switched for better impedance matching. Additionally, there is a 2.4 dB (typical) loss inside the FSWP, before the power splitter. All losses accounted for, the signal level at the power splitter input is 8.4 dBm, measured with the internal power meter. The result is shown on figure 8. The phase noise is represented as $\Re\{\langle S_{yx}\rangle\}$. The negative, invalid outcomes are replaced with $-\Re\{\langle S_{yx}\rangle\}$ and shown in different color. Because $|\Im\{\langle S_{yx}\rangle\}| \ll |\Re\{\langle S_{yx}\rangle\}|$ almost everywhere in the spectrum, $|\Re\{\langle S_{yx}\rangle\}|$ is a good approximation of $|\langle S_{yx}\rangle|$.

Scanning the 'red' region ($\Re\{\langle S_{yx}\rangle\} < 0$) of the spectrum in a frequency slot where $\Re\{\langle S_{yx}\rangle\}$ is flat and free from spurs, for example 176–325 kHz (or 465–994 kHz), we find a standard deviation $\sigma_\Re = 7\times10^{-21}$ rad^2/Hz for the real part, and $\sigma_\Im = 1.4\times10^{-20}$ rad^2/Hz for the imaginary part. The reason of this difference, not predicted by the theory stated in section 3, is not known. The quantity $\sigma_\Re$ is equivalent to a temperature deviation $\sigma_T = 3.5$ K.

5. Interpretation

The dips found at 1–1.5 kHz in figure 3, and also at 2–20 kHz in figure 6, suggest that $S_\varphi(f)$ changes sign at these points, being $S_\varphi(f) > 0$ for $f < f_{\text{dip}}$, and $S_\varphi(f) < 0$ beyond. The sign change occurs because of ςS_d in (15), related to the fact that the displayed $S_\varphi(f)$ is actually $|\langle S_{yx}(f)\rangle|$, where x and y are the phase of the DUT measured by the two channels inside the instrument. The absolute value turns the sign-change into the sharp dip observed on the log scale. This is experimentally confirmed in figure 8. By the way, the presence of such dips was already predicted by a simulation in [5, figure 1(b) and figure 3].

From a theoretical standpoint, the combined effect of the attenuator (5) and of the power splitter (18) results in

$$\mathbb{E}\{\mathsf{b}_o\} = \frac{kT_i}{P_i} + \frac{k(1-A^2)T_a}{A^2P_i} - \frac{kT_s}{A^2P_i} \tag{19}$$

at the attenuator output. This contains two systematic effects: the attenuator noise (positive), and the thermal energy of the power splitter (negative). At high attenuation ($A^2 \to 0$), the RF spectrum associated to the noise sidebands tends to kT_a. In this condition, (19) predicts $\mathsf{b}_o < 0$ because the temperature T_s inside the instrument is obviously higher than the attenuator (and room) temperature T_a.

Let us start from the oscillator $\mathcal{A}$, the old Wenzel 501-04 623E (figure 4). Using the absolute-value estimator, the

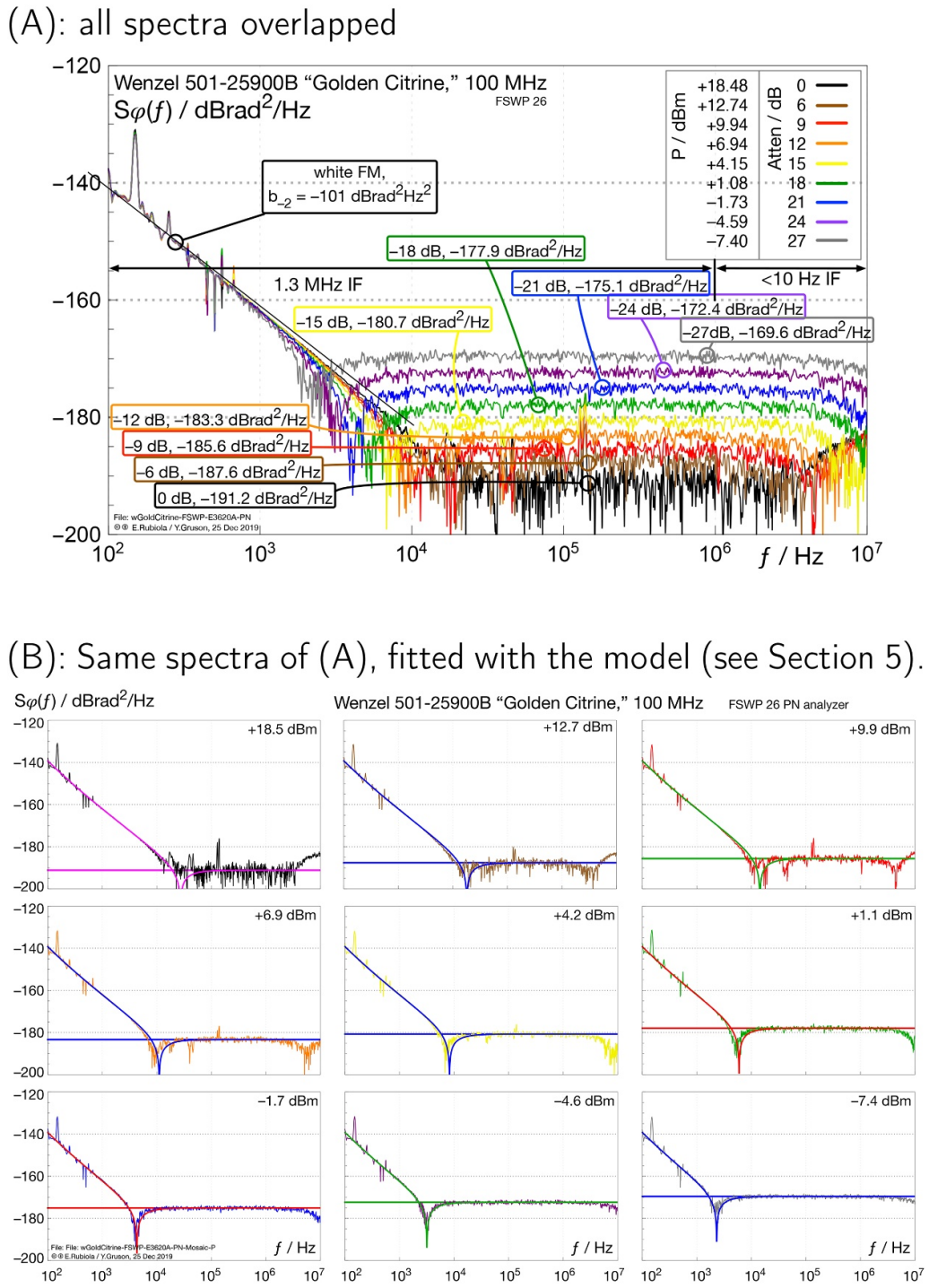

Figure 6. Phase noise of a Wenzel 501-25900B 'Golden Citrine' 100 MHz OCXO measured in the same conditions and with the same instruments of figure 3.

expected b_o is

$$\mathbb{E}\{\widehat{\mathsf{b}_o}\} = \left| \frac{kT_i}{P_i} + \frac{k(1-A^2)T_a}{A^2P_i} - \frac{kT_s}{A^2P_i} \right| . \qquad (20)$$

Fitting the experimental points with (20) fails because there results a too high T_s. Because the isolation between channels cannot be perfect, we replace T_s with $T_s - \varsigma T_c$, where ςT_c expresses the crosstalk given in terms of a temperature, and ς has the same meaning as in (15). Accordingly, (20) rewrites as

$$\mathbb{E}\{\widehat{\mathsf{b}_o}\} = \left| \frac{kT_i}{P_i} + \frac{k(1-A^2)T_a}{A^2P_i} + \frac{k(\varsigma T_c - T_s)}{A^2P_i} \right| . \qquad (21)$$

Notice that there are two unknowns in (21), T_i and $\varsigma T_c - T_s$. The former is dominant at no attenuation ($A^2 = 1$), where the observed PM noise is rather high. The latter is dominant at high

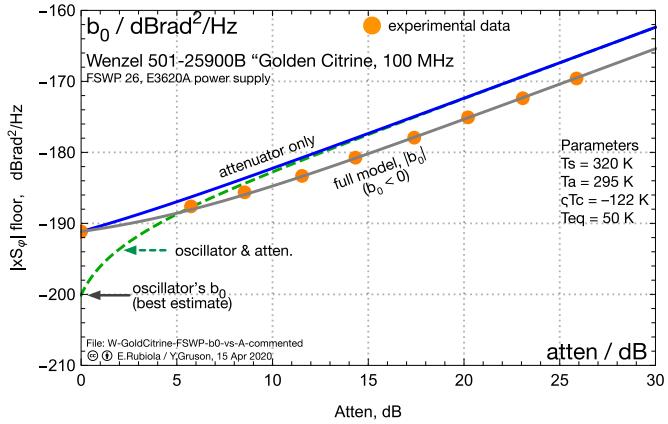

Figure 7. White noise floor b_0 (dots) taken from figure 6(A), compared to the 'attenuator only' model based on (5). The 'full model' plot and the parameters are discussed in section 5.

attenuation ($A^2 \to 0$). Because $\varsigma T_c - T_s$ appears as a single quantity in (21), separating ςT_c from T_s is somewhat artificial, but it is useful in that it provides physical insight. We assume $T_a = 295$ K (23 °C) and $T_s = 320$ K (47 °C) a convenient round number quite plausible for the instrument inside. Fitting the data of figure 4 with (21) results in $T_i = 4528$ K and $T_c = 122$ K. This is the curve labeled 'full model.' Using $\mathsf{b}_i = kT_i/P_i$, with $P_i = 9.6$ mW (+9.8 dBm at $A^2 = 1$), we get $\mathsf{b}_i = 6.5\times10^{-18}$ rad²/Hz (−171.9 dB rad²/Hz). Comparing this value to the readout (−172.4 dB rad²/Hz at $A^2 = 1$), the instrument introduces a bias of −0.5 dB due to the combined effect of power splitter and crosstalk.

Removing the absolute value in (21) yields

$$\mathbb{E}\{\widehat{\mathsf{b}_o}\} = \frac{kT_i}{P_i} + \frac{k(1-A^2)T_a}{A^2P_i} + \frac{k(\varsigma T_c - T_s)}{A^2P_i}\,, \qquad (22)$$

which results in $\mathsf{b}_o > 0$ up to 15 dB attenuation, and in $\mathsf{b}_o < 0$ beyond. Rewriting the polynomial model (1) for the absolute-value estimator we get

$$\mathbb{E}\{\widehat{S_\varphi(f)}\} = \left|\frac{\mathsf{b}_{-3}}{f^3} + \frac{\mathsf{b}_{-2}}{f^2} + \frac{\mathsf{b}_{-1}}{f} + \frac{kT_i}{P_i} + \frac{k(1-A^2)T_a}{A^2P_i} + \frac{k(\varsigma T_c - T_s)}{A^2P_i}\right|. \qquad (23)$$

Evaluating (23) with $\mathsf{b}_{-3} = 3.5\times10^{-8}$ rad² Hz² (−74.5 dB rad² Hz²), $\mathsf{b}_{-2} > 0$, and $\mathsf{b}_{-1} = 4\times10^{-14}$ dB rad² (−134 dB rad²), taken from figure 3(A), we find the solid lines overlapped to the experimental spectra of figure 3(B). The model matches the experiment, and predicts precisely the dips. These dips occur at ≥ 18 dB attenuation, where $\mathsf{b}_o < 0$. Now we turn our attention to the oscillator $\mathcal{B}$, the Wenzel 501-25900B 'Golden Citrine.' Looking at figure 6(A) and figure 7, we notice that the white noise floor increases monotonically increasing the attenuation, and the dips are present for all the values of the attenuation—albeit these dips are not clear at 0 dB and 6 dB because of insufficient averaging. This indicates that $\mathsf{b}_o < 0$ in all cases. Evaluating (23) with the same T_a, T_s and T_c as above, we find $T_{\rm osc} = T_i = 50$ K. The model fits well the experimental data, as shown on figure 7. The temperature of 50 K is equivalent to a white noise floor of −200 dB rad²/Hz at +18.5 dBm (70.5 mW) output power, with no attenuation. Finally, (23) predicts accurately the dips seen on at figure 6(B).

5.1. The origin of the crosstalk

Trying to understand the crosstalk, we look at the part of the FSWP where the strongest and the weakest signals come close to one another, which is the input mixer. Let us put numbers together with this idea. For linear conversion, the LO signal should not be lower than +20 dBm. The phase noise of a state-of the art synthesizer at 100 MHz carrier is of the order of −160 dB rad²/Hz. For reference, the R&S SMA100A synthesizer with the low-phase-noise option SMA-B22 has a white floor of this order [28, data sheet, p. 12]. At +20 dBm power, the white-noise sidebands are of −140 dBm/Hz, that is, 10^{-17} W/Hz. The crosstalk kT_c we search for is of 1.7×10^{-21} W/Hz with $T_c = 122$ K. This is 38 dB smaller than the LO sidebands. A coupling of the order of −38 dB due to leakage is quite plausible for a good mixer circuit. Besides, the absence of discontinuity in the spectrum (figure 3 and 6) at 1 MHz indicates that the crosstalk does not depend on the operating mode, which excludes some other parts of the instrument. The presence of a small amount of anticorrelated flicker PM is also possible, for the same reason. Anyway, this interpretation is just a guess, not based on the internal design nor on specific measurements.

5.2. Inside the oscillator

We address the question of the origin of $T_{\rm osc}$, and why it can be smaller than the room temperature. From our purposes, the oscillator consists of a core (the auto-oscillator in strict sense), a buffer, and an output filter (figure 9). The attenuation in the filter stopband is generally achieved by reflecting the power back to the generator's internal impedance.

The ***conventional*** oscillators may have a lowpass or bandpass RLC filter at the output to suppress the harmonic distortion and to solve other practical problems (figure 9(A)). Such filter cannot have a bandwidth smaller than a few MHz at 100 MHz carrier because the quality factor Q of these resonators is of the order of 10–20 in practical conditions. As a consequence, the output impedance is reasonably matched in the whole Fourier-frequency span, and the white noise is chiefly the noise of the sustaining amplifier, where the carrier is the weakest.

In the ***thermally limited*** quartz oscillator, a quartz resonator is present between the core and the buffer. Such filter can be the main resonator if the carrier is extracted from the resonator's ground pin [29], [30, figure 4-58 to 4-61], or a second quartz resonator (figure 9(B)). Out of the resonator bandwidth $\nu_0(1 \pm 1/2Q)$, the quartz is a high impedance circuit, thus the noise of the sustaining amplifier is not transmitted to the buffer. The noise associated to the resonator's motional resistance is also rejected, for the same reason. The buffer (a common-base amplifier) has low input impedance and low noise figure, thus the white noise is chiefly limited by the physical temperature of the collector resistor R_C at the output. Such oscillators

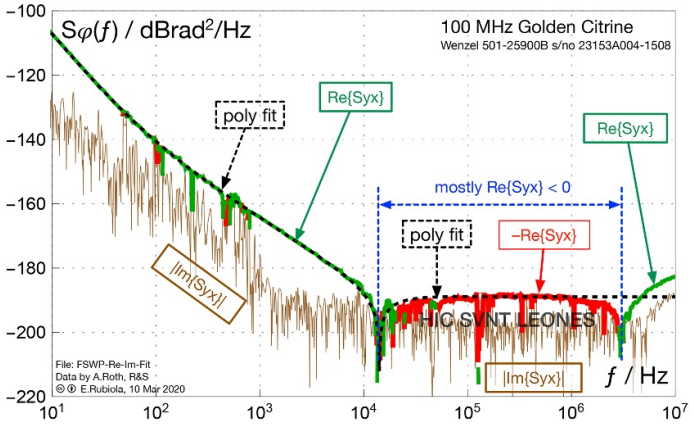

Figure 8. PM noise of a 'Golden Citrine' 100-MHz oscillator, measured with a hacked FSWP. The polynomial fit gives $\mathsf{b}_{-4} = 1.51\times10^{-7}$ rad^2 Hz^3 (-68.2 dB), $\mathsf{b}_{-3} = 3.8\times10^{-9}$ rad^2 Hz^2 (-84.2 dB), $\mathsf{b}_{-2} = 3.39\times10^{-11}$ rad^2 Hz (-104.7 dB), $\mathsf{b}_{-1} = -6.31\times10^{-16}$ rad^2 ($|\mathsf{b}_{-1}| = -152$ dB rad^2), and $\mathsf{b}_0 = -1.26\times10^{-19}$ rad^2/Hz ($|\mathsf{b}_0| = -189$ dB rad^2/Hz). The region where $\Re\{S_{yx}\} < 0$ is not a valid PM-noise spectrum, but $-\Re\{S_{yx}\}$ provides useful information related to $|S_{yx}|$ because $\Re^2\{S_{yx}\} \gg \Im^2\{S_{yx}\}$ almost everywhere. The ancient-Latin expression HIC SVNT LEONES, usually translated as 'here be dragons,' refers to an unexplored land, or to a land where humans are not permitted.

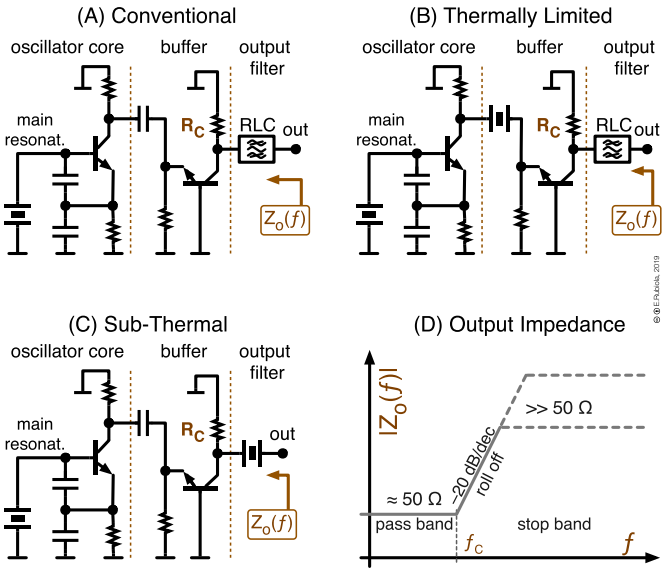

Figure 9. Simplified scheme of the low-noise quartz oscillators. The key point is the interplay of filters and impedances. Otherwise, commercial oscillators may differ from the schemes shown.

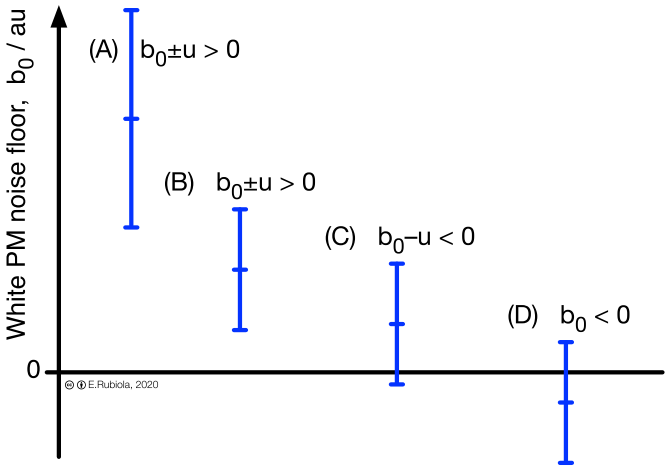

Figure 10. Uncertainty concepts, adapted from the VIM [33].

may have an additional RLC output filter of the same type discussed before.

In the ***sub-thermally limited*** quartz oscillator, a quartz resonator or a quartz filter is introduced in series to the output [31, figure 7], with no further amplification. The output filter has a small cutoff frequency even with the low Q imposed by the heavy load condition. For example, taking $Q = 5000$ at 100 MHz, the cutoff frequency is $f_c = 10$ kHz. For comparison, a good resonator at this frequency has $Q > 10^5$, unloaded. Out of the bandwidth $\nu_0(1 \pm 1/2Q)$, the output impedance is quite high ($|Z_o| \gg 50\,\Omega$), which gives the appearance of a *cold* source. There no violation of the second principle because the filter is obviously in thermal equilibrium with the environment. However, the *electrical access* to the thermal energy is open. In this condition, the input power splitter of the noise analyzer is reasonably well matched only in the pass band, and nearly open circuit in the stopband. In the stopband, the expected cross spectrum relates to the thermal energy of the power splitter (and to the crosstalk, if any), wich has negative sign in the correlation.

Simple attempts to measure the output impedance failed because the impedance analyzers do not work in the presence of the strong carrier at the input. We disassembled two 100 MHz oscillators, a Wenzel 501-04623E and a Wenzel Citrine, the same type as the oscillator $\mathcal{A}$ and $\mathcal{B}$, respectively. The oscillator $\mathcal{A}$ is of the conventional type, with a RLC filter at the output. The white PM noise limited by the signal-to-noise ratio in the sustaining amplifier. The oscillator $\mathcal{B}$ is of the sub-thermally limited type, with a quartz resonator in series to the output. Albeit we did not reverse-engineer the oscillator, the

two values of T_{osc}, 4528 K and 50 K, are consistent with the oscillator architecture.

6. Discussion

Measuring the oscillator $\mathcal{A}$, the experimentalist may be satisfied of the spectra taken with no attenuation ($A^2 = 1$) because:

- Two instruments from the major brands, with similar correlation algorithm but radically different in the RF architecture and in the detection principle, are in perfect agreement.
- The systematic error in the white noise, revealed by our rather complex experiment, is of a mere −0.5 dB, not alarming.

Conversely, the white noise floor measured on the oscillator $\mathcal{B}$ is a complete nonsense because $\Re\left\{\langle S_{yx}(f)\rangle_m\right\} < 0$ inside the instrument.

Unlike most domains of metrology (mass, length, etc), a PM noise spectrum consists of many points on the $S_\varphi(f)$ plot. The common ditto *too much information is no information* rises the question of the nature of the measurand. General experience indicates that the polynomial law (1) describes well the PM noise spectrum of quartz ad dielectric oscillators, thus a small number (4–5) of parameters b_n tell the whole story. In optics, some additional terms appear, like bumps and blue noise, which call for a small number of additional coefficients [32]. Local irregularities, like the negative spurs, can be removed after visual inspection. By contrast, an inconsistent behavior over a wide frequency range is a real problem.

Ultimately, some concepts from the International Vocabulary of Metrology (VIM) [33] and in the Guide to the Expression of Uncertainty in Measurement (GUM) [34] (see also [35, 36]) should be introduced in phase noise measurements. Going through the VIM, the following definitions are relevant to our experiments: *Type A* and *Type B* evaluation of uncertainty (2.28 and 2.29), the *influence quantities* (2.52), the *definitional uncertainty* (2.27), and the *null measurement uncertainty* (4.29). The latter concept is appropriate to describe our negative outcomes. The cases A and B of figure 10 illustrate b_0 of the oscillator $\mathcal{A}$ with small or no attenuation. The case C is likely seen increasing the attenuation, before the spectrum changes sign. D represents b_0 of the oscillators $\mathcal{B}$ and $\mathcal{C}$. The type A uncertainty u_A can be processed by a statistical analysis of the time series, or in our case of a series of spectra. Conversely, the type B uncertainty u_B can be determined by other means, chiefly the analysis of the system. The combined uncertainty (GUM section 2.3.4 and section 5) is $u_C = \sqrt{u_A^2 + u_B^2}$. In engineering, implicit reference is often made to the *expanded uncertainty* (VIM 2.35), with a coverage probability of 95 %. Because none of us is a true expert of uncertainty in metrology, subtleties may escape from our attention. However, this article shows that the assessment of uncertainty in PM noise is still at a too rudimentary stage. The *following digression* is intended to *stimulate a discussion*, with no intention of stating rules.

The single-channel background noise of the instrument is chiefly zero-average Gaussian noise with white or colored spectral distribution, thus it falls in the type A uncertainty. This can be made negligible by averaging on a sufficiently large number m of spectra. The single-channel noise is reduced by a factor of $1/\sqrt{m}$ for the absolute value estimator, and $1/\sqrt{2\,m}$ for the real-part estimator [15]. If the actual m is unclear, not well documented or hidden in algorithms, there is a trick based on the principle of ergodicity. Taking neighbor bins of the spectrum as independent random variables with nearly equal statistical properties, the *ensemble* deviation (across bins) is equal to the deviation in *time* (different realizations of the same bin, each averaged on the same m). For example, using the white noise on figure 8 and discarding the imaginary part, we get $\sigma = \sigma_\Re = 7\times10^{-21}$ rad^2/Hz (end of section 4). Adding a coverage factor, this is u_A associated of each bin. We did not try to further reduce u_A by smoothing the spectrum.

Two contributions to the type B uncertainty are obviously identified, a calibration factor and the correlated effects discussed. This suggests a minimalist model like $u_B(S_\varphi) = a_1 S_\varphi + a_0$. We have seen that the correlated white noise inside the instrument can be modeled as the temperature $\varsigma T_c - T_s$. Thus, the term a_0 is set by $\varsigma T_c - T_s$, or by the residual uncertainty if we can apply a correction. By contrast, the calibration factor a_1 is dominant on the left-hand side of the spectrum, where the white noise has no impact on $S_\varphi(f)$. Based on the $1/f^3$ noise seen on figure 3 and 5 (same oscillator, measured with two instruments of different brand, RF architecture, and principles), we infer that the uncertainty is not greater than 0.2–0.3 dB, i.e. $\lesssim 2\,\%$ in the phase-to-number conversion. The same is expected on figure 8. Such small value is not an issue in the laboratory practice, and will be neglected.

Now we look at T_s and T_c separately. Because (18) is based on simple and well-established physics, a software correction inside the instrument can compensate for T_s in a reliable way. For reference, 1 K uncertainty results in 2×10^{-22} rad^2/Hz uncertainty at $P = 70.5$ mW (oscillator $\mathcal{B}$). By contrast, there is no general way to compensate for ςT_c. We have no *a priori* reason to believe that it is a constant in the carrier-frequency range (4 decades), nor a reproducible parameter, and even the sign ς may change across different specimens of the same instrument. In our experiments, 70% of the bias error is due to the power splitter, 30% to the crosstalk. Therefore, compensating for T_s alone is a metrologically correct approach, and mitigates the problem. The brute force approach of putting the power splitter in a liquid-He cryostat [7] is not more effective because of the crosstalk.

The evaluation of $u(\varsigma T_c)$ is still not possible because we do not have enough data to provide reliable results, and the dissipative loss inside the instrument may require more attention. However, our value of T_c multiplied by a safe factor, say 2, is a good starting point for $u(\varsigma T_c)$ in similar conditions. In the absence of any indications, the upper bound of $|\varsigma T_c - T_s|$ can be *inferred* from the documentation of the instrument using $\mathsf{b}_0 = kT/P$. Thus, with a 'sensitivity' of −175 dBc/Hz (specs) or −181 dBc/Hz (typical) at 100 MHz and 10 dBm carrier, and $f = 1$ MHz (white), we find 4570 K (specs), or 1150 K (typical). This states the null measurement uncertainty of the

instrument 'out of the box,' or $u_B(T)$ if T_{eq} exceeds the calculated value.

We calculated T_{osc} for the oscillators $\mathcal{A}$ and $\mathcal{B}$, concluding that $\mathcal{B}$, could not be measured without the method proposed. Unfortunately, the $\Re$ estimator used in figure 8 is not sufficient estimate T_{osc} for the oscillator $\mathcal{C}$, nor a useful upper bound. A problem is that in München we did not measure $\varsigma T_c - T_s$ by switching the attenuation. Another problem is that the high attenuation between oscillator and power splitter (10.4 dB) obfuscates T_{osc}, hence T_{eq} is chiefly determined by the temperature of the attenuator. Equation (4) states that an error in $\varsigma T_c - T_s$ is amplified by a factor of 11 on T_{osc}.

We have seen that the output impedance $Z_o(f)$ produces erratic results if it changes significantly in the analysis bandwidth. This opens the question of whether $Z_o(f)$ goes in the definitional uncertainty (it is inside the DUT), it goes in the B-type uncertainty, or if it is an influence quantity. The role of impedance mismatch is well known in microwave noise measurements [37, 38], but these concepts have not been transposed to PM noise.

Finally, we want to draw the attention to the vertues of the real-part estimator $\Re\left\{\langle S_{yx}\rangle_m\right\}$. It is superior to the traditional estimator $\left|\langle S_{yx}\rangle_m\right|$ in that (i) it converges faster because the background noise in $\Im\left\{\langle S_{yx}\rangle_m\right\}$ is not taken in, and (ii) it reveals the negative, nonsensical outcomes.

7. Conclusions

Our method consists of introducing various values of dissipative attenuation between the oscillator under test and the phase-noise analyzer. This method is new. It provides quantitative information about the unwanted correlated effects inside the analyzer, and helps to assess the null measurement uncertainty, i.e. the minimum amount of phase noise that can be detected. In some circumstances, inserting an attenuator results in lower white PM noise floor. When this happens, gross errors are around the corner. The idea that the (anti-)correlated noise inside the instrument can be described in terms of the thermal energy $k(\varsigma T_c - T_s)$ is also new. This parameter accounts for the temperature of the power splitter at the instrument input, and the crosstalk between the two channels.

The experiments described provide the evidence that pushing the noise rejection too far by averaging on a large number of data may result in misleading or grossly wrong results. The reason is in residual correlated effects, not under control. In general terms, under-estimating the DUT noise is obviously worse than over-estimating it.

Impedance matching in the whole analysis bandwidth is a critical issue. Sub-thermally limited oscillators make use of a narrowband reactive filter at the output, which exploits impedance mismatch in the stopband to deliver the lowest noise floor. However, such filter results in anticorrelated noise due to the thermal energy in the power splitter at the instrument input. From a different standpoint, the benefit of a sub-thermally limited oscillator is unclear to us if the oscillator is intended to be a part of a system at room temperature.

Disclaimer

Our strong statements require an equally strong disclaimer about the commercial products we refer to. We experimented on them because they were on hand at the right time, as opposite to gathering parts with this research in mind. By no means we criticize these products, nor we endorse them. The problems and the inconsistencies we describe relate to unintended, strange, or weird use of these products. Driven by the genuine scientific curiosity, we share our knowledge with the ultimate intent to contribute to better understanding the physics and the technology of phase noise metrology. We hope that no misunderstanding will arise, and we apologize if this will happen.

Acknowledgments

This work is funded by the ANR Programme d'Investissement d'Avenir under the Oscillator IMP project (contract ANR-11-EQPX-0033-OSC-IMP) and the FIRST-TF network (contract ANR-10-LABX-48-01), and by the Région Bourgogne Franche Comté. We thank AR Electronique (the similarity between this brand and the initials of one of the authors is a random outcome), Besançon, for hosting us in their R&D lab for some additional measurements, and Cristian Bolovan and Radu Ohreac, Rohde & Schwarz Romania, for generously lending a FSWP 8.

ORCID iD

Enrico Rubiola https://orcid.org/0000-0002-5364-1835

References

[1] Walls F L, Stain S R, Gray J E and Glaze D J 1976 Design considerations in state-of-the-art signal processing and phase noise measurement systems *Proc. Freq. Control Symp.* Atlantic City, NJ, USA pp 269–74
[2] Walls W F 1992 Cross-correlation phase noise measurements *Proc. Freq. Control Symp.* Hershey, PA pp 257–61
[3] Rubiola E and Giordano V 2000 Correlation-Based Phase Noise Measurements *Rev. Sci. Instrum.* **71** 3085–91
[4] Ivanov E N and Walls F L 2002 Interpreting anomalously low voltage noise floors in two-channel measurement systems *IEEE Trans. Ultras. Ferroelec. Freq. Contr.* **49** 11–19
[5] Nelson C W, Hati A and Howe D A 2014 A collapse of the cross-spectral function in phase noise metrology *Rev. Sci. Instrum.* **85** 024705
[6] Hati A, Nelson C W and Howe D A 2016 Cross-spectrum measurement of thermal-noise limited oscillators *Rev. Sci. Instrum.* **87** 034708
[7] Hati A, Nelson C W, Pappas D P and Howe D A 2017 Phase noise measurements with a cryogenic power-splitter to minimize the cross-spectral collapse effect *Rev. Sci. Instrum.* **88** 114707
[8] Breitbarth J 2013 Source impedance influence on cross-correlation phase noise measurements *Proc. Intl. Freq. Control Symp. and Europ. Freq. Time Forum Joint Meeting* Prague, Czech Republic 434–7
[9] *Cross Spectrum $\mathcal{L}(f)$ Workshop* 2017 *Besançon, France Side event at the 2017 Europ. Freq. Time Forum and Freq. Symp. Joint Meeting* pp 10–13

[10] *Cross Spectrum $\mathscr{L}(f)$ Workshop* 2015 *Denver, CO, USA Side event at the 2015 Europ. Freq. Time Forum and Freq. Symp.Joint Meeting* pp 13–16

[11] *European Workshop on Cross-Spectrum Phase Noise Measurements* 2014 Laboratoire National de métrologie et d'Essays (LNE) Paris, France

[12] Ferre-Pikal E S 2009 *IEEE Standard Definitions of Physical Quantities for Fundamental Frequency and Time Metrology–Random Instabilities (IEEE Standard 1139-2008)* (New York: IEEE) (PDF) https://doi.org/10.1109/ieeestd.2009.6581834

[13] Tiuri M E 1966 Radio-Telescope Receivers Chap 7 J D Kraus *Radio Astronomy* (New York: McGraw Hill)

[14] Rohlfs K and Wilson T L 2000 *Tools of Radio Astronomy* (Berlin, Heidelberg, New York: Springer)

[15] Rubiola E and Vernotte F 2010 *The Cross-Spectrum Experimental Method* arXiv:1003.0113 [physics.ins-det]

[16] Sampietro M, Fasoli L and Ferrari G 1999 Spectrum Analyzer with Noise Reduction by Cross-Correlation Technique on Two Channels *Rev. Sci. Instrum.* **70** 2520–5

[17] Feldhaus G and Roth A 2016 A 1 MHz to 50 GHz Direct Down-Conversion Phase Noise Analyzer with Cross-Correlation *Proc. Freq. Control Symp.* York, UK https://doi.org/10.1109/eftf.2016.7477759

[18] Gruson Y, Giordano V, Rohde U L, Poddar A K and Rubiola E 2017 Cross-Spectrum PM Noise Measurement, Thermal Energy and Metamaterial Filters *IEEE Trans. Ultras. Ferroelec. Freq. Contr.* **64** 634–42

[19] Rubiola E 2007 The effect of AM noise on correlation phase noise measurements *IEEE Trans. Ultras. Ferroelec. Freq. Contr.* **54** 926–32 Also arXiv: physics/0609147

[20] Fischer J 2015 Progress towards a new definition of the kelvin *Metrologia* **52** S364–S375

[21] White D R 1996 The status of Johnson noise thermometry *Metrologia* **33** 325–35

[22] Allred C M 1962 A Precision Noise Spectral Density Comparator *J. Res. NBS* **66C** 323–30

[23] Halford G J 1966 Noise Comparators for S and X Bands *IEEE Trans. Instrum. Meas.* **15** 310–17

[24] Rohde & Schwarz 2019 *R& S FSWP Phase Noise Analyzer and VCO Tester Brochures and Data Sheets available on* https://www.rohde-schwarz.com/us/brochure-datasheet/fswp/ accessed December 21

[25] Rohde U L, Whitaker J C and Zahnd H 2017 *Communications Receivers* 4th (New York: Mc Graw Hill Education)

[26] Keysight Technologies 2019 *E5500 Series, Phase Noise Measurement Solutions* available on https://www.keysight.com/us/en/assets/7018-01214/data-sheets/5989-0851.pdf accessed December 21

[27] Wenzel Associates 2019 *Low Noise Crystal Oscillators > VHF Citrine* brochure available on www.wenzel.com/wp-content/uploads/VHF-Citrine.pdf accessed December 21

[28] Rohde & Schwarz 2019 *R&S SMA100A Signal Generator* Brochures and Data Sheets available on https://www.rohde-schwarz.com/us/brochure-datasheet/sma100a/ accessed December 21

[29] Rohde U L 1975 Crystal oscillator provides low noise *Electron. Des.* **21**

[30] Rohde U L 1997 *Microwave and Wireless Synthesizers* (New York: Wiley)

[31] Rohde U L 1978 Mathematical Analysis and Design of Ultra Stable Low Noise 100 MHz Crystal Oscillator with Differential Limiter and its Possibilities in Frequency Standards *Proc. Freq. Control Symp.* pp 409–25

[32] Calosso C E, Clivati C and Micalizio S 2016 Avoiding Aliasing in Allan Variance: An Application to Fiber Link Data Analysis *IEEE Trans. Ultras. Ferroelec. Freq. Contr.* **63** 646–55

[33] Joint Committee for Guides in Metrology (JCGM) 2012 *Int. Vocabulary of Metrology — Basic and General Concepts and Associated Terms (VIM), document JCGM* Available on https://www.bipm.org/en/publications/guides/ vol 200

[34] Joint Committee for Guides in Metrology (JCGM) 2008 *Evaluation of measurement data —- Guide to the expression of uncertainty in measurement (GUM), document JCGM* Available on https://www.bipm.org/en/publications/guides/ vol 1008

[35] Hall B D 2016 Evaluating the measurement uncertainty of complex quantities: a selective review *Metrologia* **53** S25–S31

[36] Possolo A and Iyer H K 2017 Concepts and tools for the evaluation of measurement uncertainty *Rev. Sci. Instrum.* **88** 011301

[37] Otoshi T Y 1968 The Effect of Mismatched Components on Microwave Noise-Temperature Calibrations *IEEE Trans. Microw. Theory Tech.* **16** 675–86

[38] Wedge S M and Rutledge D B 1992 Wave Techniques for Noise Modeling and Measurement *IEEE Trans. Microw. Theory Tech.* **40** 2004–12

Artifacts and errors in cross-spectrum phase noise measurements